SOLAR NEUTRINO RESULTS FROM SUPER-KAMIOKANDE

YASUO TAKEUCHI
for the Super-Kamiokande Collaboration
Kamioka Observatory, ICRR, Univ. of Tokyo,
Higashi-Mozumi, Kamioka-cho, Yoshiki-gun, Gifu 506-1205, Japan
E-mail: takeuchi@icrr.u-tokyo.ac.jp

ABSTRACT

The solar neutrino results from 1258days of measurement from Super-Kamiokande are reported.

1. Super-Kamiokande

Super-Kamiokande is a large cylindrical imaging water Čerenkov detector, which is constructed from 50000 ton of pure water, 11146 of 20 inch PMTs, 1867 of 8 inch PMTs, and so on. It is located at Kamioka Observatory, Institute for Cosmic Ray Research, University of Tokyo about 1000m underground (2700m water equivalent) in the Mozumi mine in Kamioka. The detection method for Solar neutrinos in Super-Kamiokande is:

$$\nu + \mathrm{e}^- \rightarrow \mathrm{e}^- + \nu.$$

The detector observes the Čerenkov photons radiated from the recoil electron in the water. Detailed descriptions of Super-Kamiokande detector can be found elsewhere [1,2,3,4,5,6,7,8].

2. Data Analysis

Table 1 shows a summary of the trigger thresholds, analysis energy thresholds, and live-times for the latest solar neutrino data set. The total live-time of the latest solar neutrino data set is 1258 days. The 1258-day solar neutrino data were collected in four periods with different trigger thresholds between May 31, 1996 and October 6, 2000. The current analysis energy threshold of Super-Kamiokande is 5.0MeV.

Run period	50/95% efficiency (MeV)	Analysis threshold (MeV)	Live-time (days)
(1) May 1996 ∼	5.7 / 6.2	6.5	280
(2) May 1997 ∼	4.7 / 5.2	5.0	650
(3) Sep. 1999 ∼	4.2 / 4.6	5.0	320
(4) Sep. 2000 ∼	3.7 / 4.2	5.0	8

Table 1: The trigger and analysis thresholds and live-times during which they were used. The 2nd column shows the recoil electron energy at which the trigger is 50% and 95% efficient.

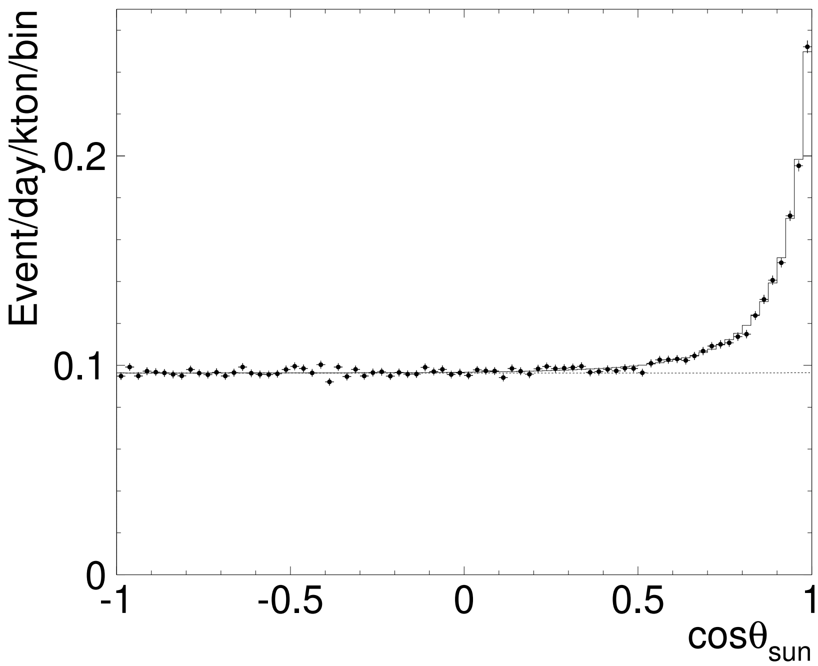

Figure 1: $\cos\theta_{\text{sun}}$ distribution for reconstructed energy $E = 5.0$–20.0 MeV. The points represent observed data, the histogram shows the best-fit signal level plus background, and the nearly horizontal line shows the estimated background. The peak at $\cos\theta_{\text{sun}} = 1$ is due to solar neutrinos.

In order to obtain solar neutrino signals, we apply an extended maximum likelihood method using the angle between the recoil electron momentum and the vector from the sun to the earth. This angle is defined as θ_{sun}. Figure 1 shows the $\cos\theta_{\text{sun}}$ distribution of the 1258 days final data sample with 5.0–20MeV recoil electron energy. The solar neutrino flux is obtained by the likelihood fit of the signal and background shapes to the $\cos\theta_{\text{sun}}$ distribution in data. The likelihood function is defined as follows:

$$\mathcal{L} = \prod_{j=1}^{N_{ene}} \frac{e^{-(B_j+S_j)}}{N_j!} \prod_{i=1}^{N_j} [B_j \cdot F_b(\cos\theta_{\text{sun},i}, E_i) + S_j \cdot F_s(\cos\theta_{\text{sun},i}, E_i)]$$

$$S_j = Y_j \cdot S$$

Here, N_{ene} is the total number of energy bins, while N_j, B_j, S_j, and Y_j represent the number of observed events, the number of background events (parameters to be fitted), the number of signal events, and the expected fraction of signal events in the j-th energy bin, respectively. S is a single parameter for the total number of signal events. F_b and F_s are the probability for the background and signal events as a function of $\cos\theta_{\text{sun}}$ and energy (E_i) of each event. The likelihood function is maximized with respect to S and B_j. We use BP2000 SSM [9)a] and Ortiz *et al.* [10)]

[a]The ^{8}B flux used in this report is 5.15×10^6 cm^{-2} s^{-1}. After the analysis was finished, we were informed that the ^{8}B flux has been updated to 5.05×10^6 cm^{-2} s^{-1} in BP2000 SSM.

^{8}B spectrum as the standard reference. For the energy spectrum measurement, each term in the product over energy bins is maximized separately.

3. Results

The best-fit value of solar neutrino signal is $18,464 \pm 204$ (stat.)$^{+646}_{-554}$ (sys.), which is 45.1 $\pm$ 0.5 (stat.) $^{+1.6}_{-1.4}$ (sys.)% of the reference prediction. The corresponding ^{8}B flux at 1 AU is:

$$2.32 \pm 0.03 \text{ (stat.)}^{+0.08}_{-0.07} \text{ (sys.)} \times 10^6 \text{ cm}^{-2}\text{s}^{-1}.$$

The day-time solar neutrino flux Φ_d is defined as the flux of events when $\cos\theta_z \leq 0$, while the night-time flux Φ_n is that when $\cos\theta_z > 0$. The measured fluxes are:

$$\begin{aligned} \Phi_d &= 2.28 \pm 0.04 \text{ (stat.)}^{+0.08}_{-0.07} \text{ (sys.)} \times 10^6 \text{ cm}^{-2}\text{s}^{-1} \\ \Phi_n &= 2.36 \pm 0.04 \text{ (stat.)}^{+0.08}_{-0.07} \text{ (sys.)} \times 10^6 \text{ cm}^{-2}\text{s}^{-1} \end{aligned}$$

Including systematic errors, this is 1.3 σ from zero asymmetry. Figure 2 shows the solar zenith angle (θ_z) dependence of the solar neutrino flux. The θ_z is defined as the angle between the vertical axis at SK and the vector from the sun to the earth.

Figure 3 shows the measured recoil electron energy spectrum. A fit to an undistorted energy spectrum gives $\chi^2/d.o.f. = 19.1/18$. Energy-correlated systematic errors are considered in the definition of χ^2 [3]. The energy-correlated systematic error, which is shown in Fig. 3 as a band around the total flux, is due to uncertainties that could cause a systematic shift in the energy spectrum.

Figure 4 shows the seasonal dependence of the solar neutrino flux. The points represent the measured flux, and the curve shows the expected variation due to the orbital eccentricity of the earth (assuming no neutrino oscillations, and normalized to the measured total flux). The data are consistent with the expected annual variation with $\chi^2/d.o.f. = 3.9/7$. A fit to a flat distribution gives $\chi^2/d.o.f. = 8.1/7$. Systematic errors are included in the calculation of χ^2.

4. Oscillation analysis

Using the 1258 days of solar neutrino data in Super-Kamiokande, we have performed a search for neutrino oscillations. The data sample is divided into seven solar zenith angle bins; within each zenith angle bin, the data are divided into eight energy bins. From the statistical limitation, the lowest (5.0-5.5 MeV) and the highest (16.0-20.0 MeV) energy bin combine the flux of all zenith angles. Table 2 shows the obtained solar neutrino fluxes for all solar zenith angle and energy bins. The probability of two neutrino oscillation scenarios was tested with a χ^2 method. The detailed description about this oscillation analysis is reported in Ref. [8].

Figure 5 shows the result of the two-flavor oscillation analysis for active neutrinos. The shaded areas in Fig. 5 are excluded at 95% C.L. from the flux-independent

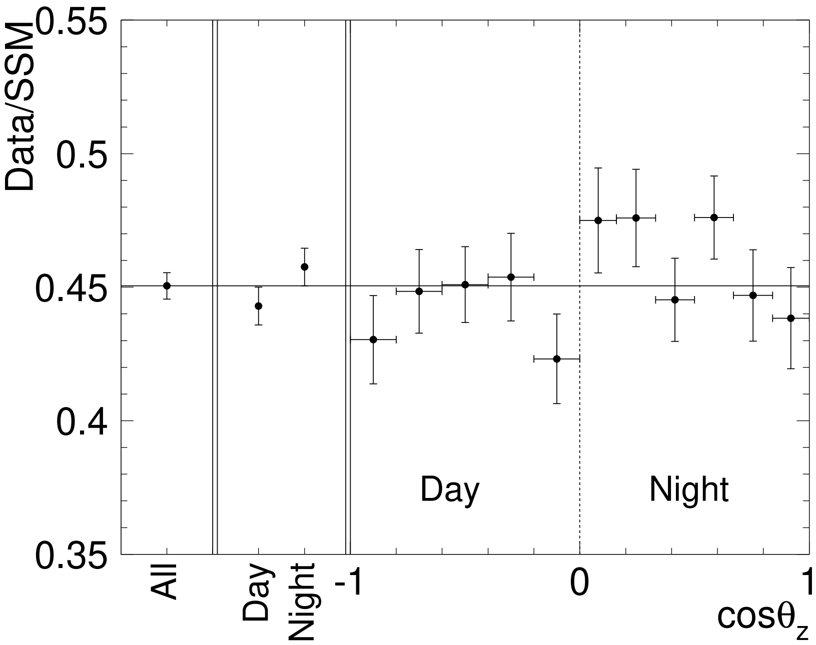

Day-Night	Solar zenith angle	Data/SSM	δ_i
DAY	$-1 \leq \cos\theta_z \leq 0$	$0.443^{+0.007}_{-0.007}$	——
MAN1	$0 < \cos\theta_z \leq 0.16$	$0.475^{+0.020}_{-0.020}$	$^{+1.3}_{-1.2}\%$
MAN2	$0.16 < \cos\theta_z \leq 0.33$	$0.476^{+0.018}_{-0.018}$	$^{+1.3}_{-1.2}\%$
MAN3	$0.33 < \cos\theta_z \leq 0.50$	$0.445^{+0.016}_{-0.016}$	$^{+1.3}_{-1.2}\%$
MAN4	$0.50 < \cos\theta_z \leq 0.67$	$0.476^{+0.016}_{-0.016}$	$^{+1.3}_{-1.2}\%$
MAN5	$0.67 < \cos\theta_z \leq 0.84$	$0.447^{+0.017}_{-0.017}$	$^{+1.3}_{-1.2}\%$
CORE	$0.84 < \cos\theta_z \leq 1$	$0.438^{+0.019}_{-0.019}$	$^{+1.3}_{-1.2}\%$

Figure 2: The solar zenith angle dependence of the solar neutrino flux. Energy range is 5.0–20.0MeV. The width of the night-time bins was chosen to separate solar neutrinos that pass through the Earth's core ($\cos\theta_z \geq 0.84$) from those that pass through the mantle ($0 < \cos\theta_z < 0.84$). The error bars in the plot show statistical error. The 4th column of the table is 1σ error of systematic error. Systematic errors are relative to Day-flux.

Day-Night	DAY	MAN1	MAN2	MAN3	MAN4	MAN5	CORE
5.0–5.5 MeV				0.436±0.046			
5.5–6.5 MeV	0.431±0.022	0.464±0.060	0.410±0.055	0.442±0.048	0.453±0.048	0.495±0.054	0.434±0.058
6.5–8.0 MeV	0.461±0.013	0.524±0.036	0.506±0.033	0.438±0.028	0.466±0.027	0.424±0.030	0.409±0.033
8.0–9.5 MeV	0.437±0.014	0.449±0.038	0.482±0.036	0.460±0.031	0.503±0.031	0.461±0.034	0.439±0.037
9.5–11.5 MeV	0.434±0.015	0.432±0.042	0.493±0.040	0.446±0.034	0.448±0.034	0.435±0.037	0.484±0.044
11.5–13.5 MeV	0.456±0.026	0.496±0.071	0.290±0.055	0.394±0.053	0.477±0.056	0.439±0.061	0.465±0.068
13.5–16.0 MeV	0.482±0.056	0.532±0.155	0.775±0.171	0.685±0.141	0.607±0.130	0.471±0.128	0.539±0.153
16.0–20.0 MeV				0.476±0.149			

Table 2: The solar neutrino flux results for the "zenith angle spectrum" oscillation analysis. The definitions of Day-Night is same as the table in Fig. 2. The zenith angle bin of the lowest and the highest energy bin are combined because of statistical limitation.

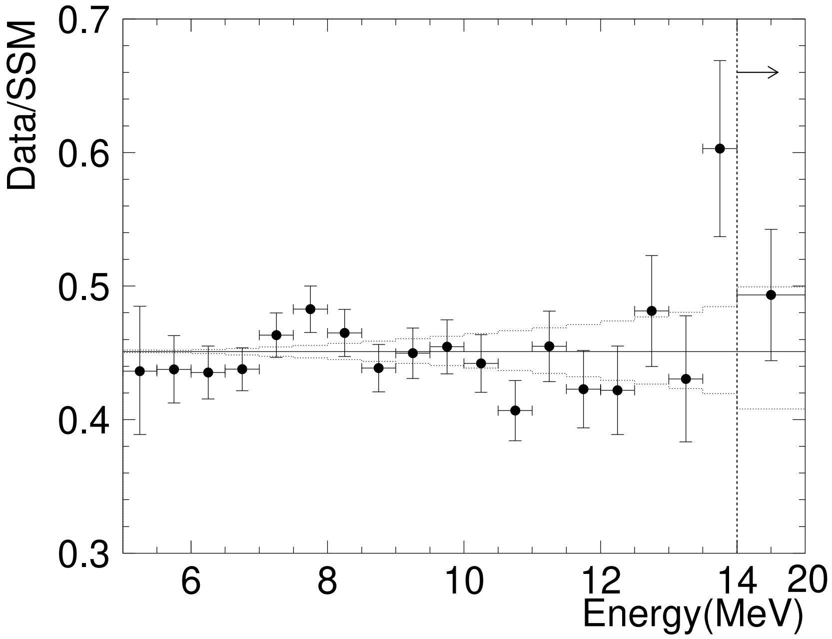

Energy	Data/SSM			$\delta_{i,cor.}$	$\delta_{i,uncor.}$
(MeV)	ALL	DAY	NIGHT		
5.0-5.5	$0.436^{+0.046}_{-0.046}$	$0.438^{+0.065}_{-0.065}$	$0.434^{+0.063}_{-0.063}$	$^{+0.2}_{-0.2}\%$	$^{+3.9}_{-3.1}\%$
5.5-6.0	$0.438^{+0.024}_{-0.024}$	$0.428^{+0.034}_{-0.034}$	$0.446^{+0.034}_{-0.034}$	$^{+0.2}_{-0.2}\%$	$^{+1.7}_{-1.6}\%$
6.0-6.5	$0.435^{+0.019}_{-0.019}$	$0.426^{+0.027}_{-0.027}$	$0.444^{+0.027}_{-0.027}$	$^{+0.3}_{-0.3}\%$	$^{+1.3}_{-1.4}\%$
6.5-7.0	$0.438^{+0.015}_{-0.015}$	$0.431^{+0.021}_{-0.021}$	$0.444^{+0.021}_{-0.021}$	$^{+0.5}_{-0.6}\%$	$^{+1.4}_{-1.4}\%$
7.0-7.5	$0.463^{+0.015}_{-0.015}$	$0.462^{+0.022}_{-0.022}$	$0.464^{+0.022}_{-0.022}$	$^{+0.8}_{-0.8}\%$	$^{+1.3}_{-1.4}\%$
7.5-8.0	$0.483^{+0.016}_{-0.016}$	$0.494^{+0.023}_{-0.023}$	$0.472^{+0.022}_{-0.022}$	$^{+1.0}_{-1.1}\%$	$^{+1.3}_{-1.4}\%$
8.0-8.5	$0.465^{+0.017}_{-0.017}$	$0.452^{+0.023}_{-0.023}$	$0.477^{+0.023}_{-0.023}$	$^{+1.4}_{-1.3}\%$	$^{+1.3}_{-1.4}\%$
8.5-9.0	$0.438^{+0.017}_{-0.017}$	$0.402^{+0.024}_{-0.024}$	$0.473^{+0.024}_{-0.024}$	$^{+1.7}_{-1.7}\%$	$^{+1.3}_{-1.4}\%$
9.0-9.5	$0.450^{+0.018}_{-0.018}$	$0.454^{+0.026}_{-0.026}$	$0.446^{+0.025}_{-0.025}$	$^{+2.1}_{-2.0}\%$	$^{+1.3}_{-1.4}\%$
9.5-10.0	$0.455^{+0.019}_{-0.019}$	$0.449^{+0.027}_{-0.027}$	$0.460^{+0.027}_{-0.027}$	$^{+2.5}_{-2.3}\%$	$^{+1.3}_{-1.4}\%$
10.0-10.5	$0.442^{+0.021}_{-0.021}$	$0.430^{+0.029}_{-0.029}$	$0.454^{+0.029}_{-0.029}$	$^{+3.0}_{-2.7}\%$	$^{+1.3}_{-1.4}\%$
10.5-11.0	$0.407^{+0.022}_{-0.022}$	$0.386^{+0.030}_{-0.030}$	$0.426^{+0.032}_{-0.032}$	$^{+3.4}_{-3.2}\%$	$^{+1.3}_{-1.4}\%$
11.0-11.5	$0.455^{+0.026}_{-0.026}$	$0.439^{+0.036}_{-0.036}$	$0.470^{+0.037}_{-0.037}$	$^{+3.9}_{-3.6}\%$	$^{+1.3}_{-1.4}\%$
11.5-12.0	$0.423^{+0.028}_{-0.028}$	$0.455^{+0.042}_{-0.042}$	$0.394^{+0.038}_{-0.038}$	$^{+4.5}_{-4.2}\%$	$^{+1.3}_{-1.4}\%$
12.0-12.5	$0.422^{+0.033}_{-0.033}$	$0.389^{+0.045}_{-0.045}$	$0.455^{+0.047}_{-0.047}$	$^{+5.1}_{-4.8}\%$	$^{+1.3}_{-1.4}\%$
12.5-13.0	$0.481^{+0.041}_{-0.041}$	$0.514^{+0.061}_{-0.061}$	$0.451^{+0.055}_{-0.055}$	$^{+5.8}_{-5.4}\%$	$^{+1.3}_{-1.4}\%$
13.0-13.5	$0.431^{+0.047}_{-0.047}$	$0.468^{+0.070}_{-0.070}$	$0.397^{+0.063}_{-0.063}$	$^{+6.5}_{-6.2}\%$	$^{+1.3}_{-1.4}\%$
13.5-14.0	$0.603^{+0.065}_{-0.065}$	$0.551^{+0.092}_{-0.092}$	$0.653^{+0.094}_{-0.094}$	$^{+7.4}_{-7.0}\%$	$^{+1.3}_{-1.4}\%$
14.0-20.0	$0.493^{+0.049}_{-0.049}$	$0.430^{+0.067}_{-0.067}$	$0.559^{+0.071}_{-0.071}$	$^{+10.7}_{-9.5}\%$	$^{+1.3}_{-1.4}\%$

Figure 3: The measured solar neutrino spectrum. The plot and table show the spectrums in all-time and in all/day/night-time, respectively. The data from 14 MeV to 20 MeV are combined into a single bin. The horizontal solid line in the plot shows the measured total flux, while the dotted band around this line indicates the energy correlated uncertainty. Error bars in the plot show statistical and energy-uncorrelated errors added in quadrature. Error of 2nd, 3rd, and 4th column in the table show only statistical errors. The 5th and 6th column in the table show 1σ error of correlated systematic error and 1σ error of uncorrelated systematic error, respectively. Systematic errors are relative.

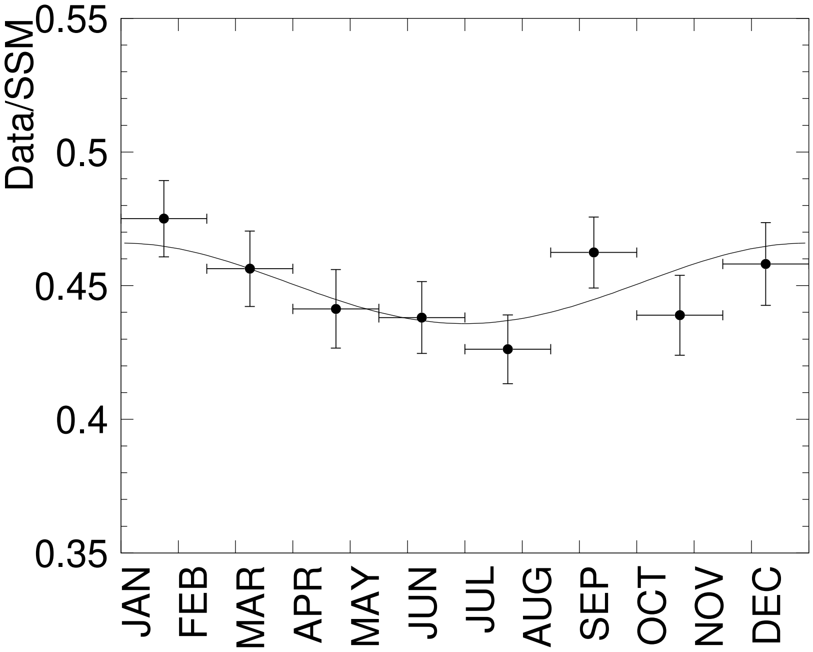

Time period	Data/SSM	Data/SSM at 1 AU	δ_i
Jan. 1 – Feb. 16	$0.475^{+0.014}_{-0.014}$	$0.461^{+0.014}_{-0.014}$	$^{+1.3}_{-1.3}\%$
Feb. 17 – Apr. 2	$0.456^{+0.014}_{-0.014}$	$0.450^{+0.014}_{-0.014}$	$^{+1.3}_{-1.3}\%$
Apr. 3 – May 19	$0.441^{+0.015}_{-0.015}$	$0.446^{+0.015}_{-0.015}$	$^{+1.3}_{-1.3}\%$
May 20 – Jul. 4	$0.438^{+0.013}_{-0.013}$	$0.451^{+0.014}_{-0.014}$	$^{+1.3}_{-1.3}\%$
Jul. 5 – Aug. 19	$0.426^{+0.013}_{-0.013}$	$0.439^{+0.013}_{-0.013}$	$^{+1.3}_{-1.3}\%$
Aug. 20 – Oct. 4	$0.462^{+0.013}_{-0.013}$	$0.469^{+0.014}_{-0.014}$	$^{+1.3}_{-1.3}\%$
Oct. 5 – Nov. 18	$0.439^{+0.015}_{-0.015}$	$0.434^{+0.015}_{-0.015}$	$^{+1.3}_{-1.3}\%$
Nov. 19 – Dec. 31	$0.458^{+0.016}_{-0.016}$	$0.445^{+0.015}_{-0.015}$	$^{+1.3}_{-1.3}\%$

Figure 4: Seasonal variation of the solar neutrino flux. Energy range is 5.0–20.0MeV. The curve shows the expected seasonal variation of the flux introduced by the eccentricity of the earth's orbit. Error bars show statistical errors only. The 2th, 3rd, and 4th column of the table show the ratio of observed and expected number of events without eccentricity correction, the ratio of observed and expected number of events with eccentricity correction, and 1σ error of systematic error, respectively. Systematic errors are relative.

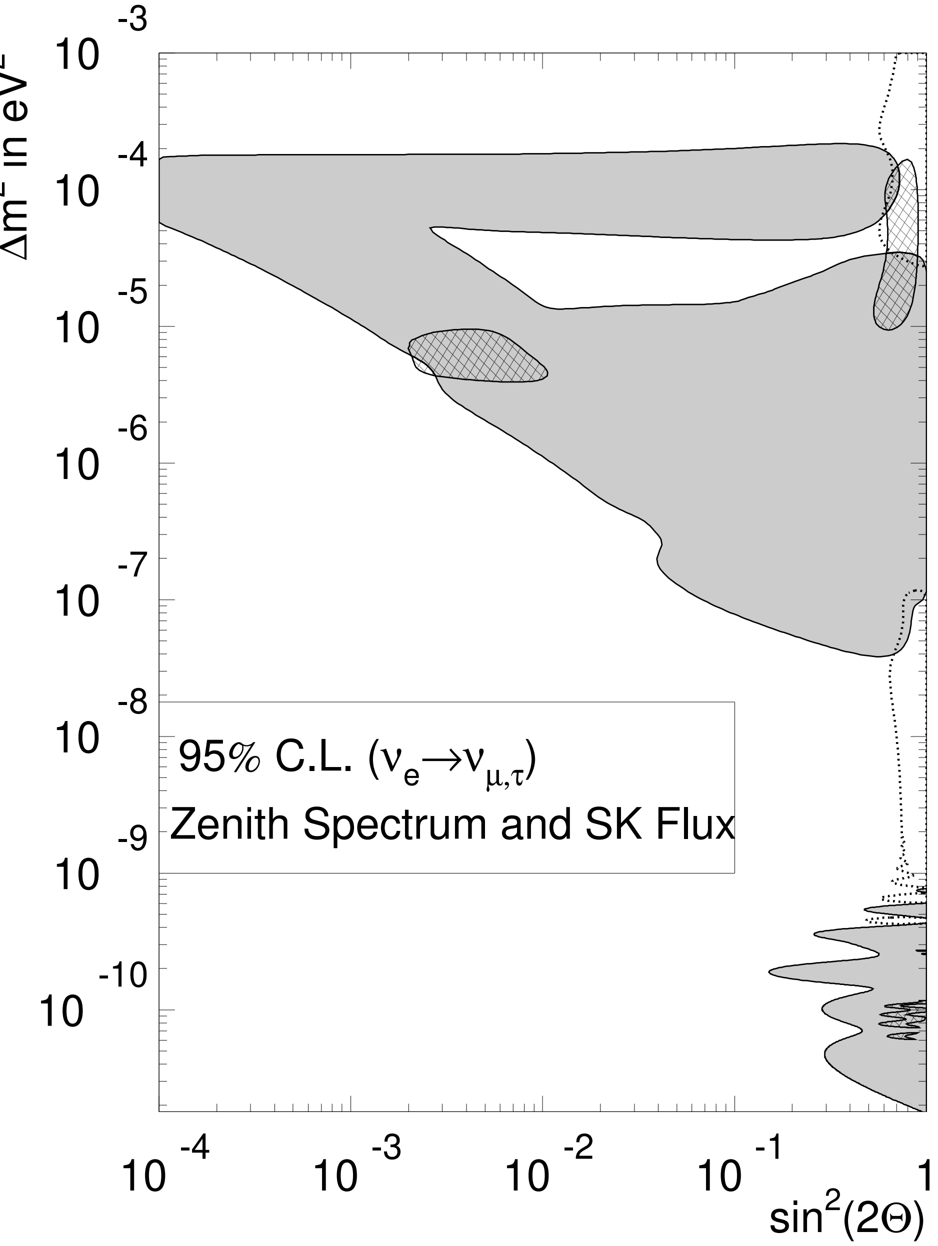

Figure 5: Exclusion area for two-flavor oscillation $\nu_e \leftrightarrow \nu_\mu/\nu_\tau$ from (flux-independent) zenith angle spectrum analysis at 95% confidence level (gray areas). The *hep* contribution to the neutrino flux is not constrained. Overlaid are the allowed areas (95% C.L.) obtained by the flux-constraint analysis using the zenith angle spectrum and the SSM flux prediction (inside dotted lines). The cross-hatched areas are allowed at 95% in a combined fit based only on the absolute fluxes measured at GALLEX[13)], SAGE[12)], Homestake[11)] and Super-Kamiokande[7)].

analysis using the zenith angle spectrum data in Table 2. Most of the SMA and just-so solutions are disfavored with this C.L.. The minimum χ^2 value is 36.1 with 40 degrees of freedom at ($\sin^2 2\theta = 1$, $\Delta m^2 = 6.53 \cdot 10^{-10}$ eV^2).

The dotted lines in Fig. 5 show the contours of the 95% C.L. allowed regions from an analysis combining ^{8}B flux and zenith angle spectrum. The minimum χ^2 value is 37.8 with 41 d.o.f. at the same position as the unconstrained case. Some LMA χ^2 are similar to the minimum. For example, $\chi^2 = 39.1$ at ($\sin^2 2\theta = 0.87, \Delta m^2 = 7 \cdot 10^{-5}$ eV^2).

5. Summary

Solar neutrino measurements from 1258 days of data from the Super-Kamiokande detector are reported. The measurements are based on recoil electrons in the energy range 5.0–20.0 MeV, and the data were collected between May 31, 1996 and October 6, 2000. The measured solar neutrino flux is 2.32$\pm$0.03 (stat.) $^{+0.08}_{-0.07}$ (sys.) $\times 10^6$ cm^{-2} s^{-1}, which is 45.1 $\pm$ 0.5 (stat.) $^{+1.6}_{-1.4}$ (sys.)% of that predicted by the BP2000 SSM. The seasonal dependence of the flux shows the expected 7% annual variation due to the eccentricity of the earth's orbit. We found no statistically significant energy spectrum distortion ($\chi^2/d.o.f. = 19.1/18$ relative to the predicted ^{8}B spectrum), and the day-night flux difference of 3.3% of the average flux is 1.3 σ from zero. However, the absence of significant zenith angle variation and spectrum distortion places strong constraints on neutrino mixing and mass difference in a flux-independent way. Using the Super-Kamiokande flux measurement in addition, two allowed areas at large mixing remain. For the active neutrino case, one of these allowed area overlaps with the LMA solution, the other one stretches from 10^{-7} to 10^{-10} eV^2.

6. Acknowledgments

The author acknowledges the cooperation of the Kamioka Mining and Smelting Company. The Super-Kamiokande detector has been built and operated from funding by the Japanese Ministry of Education, Culture, Sports, Science and Technology, the U.S. Department of Energy, and the U.S. National Science Foundation. This work was supported in part by Grant-in-Aid for Scientific Research (B) of the Japanese Ministry of Education, Culture, Sports, Science and Technology.

7. References

1) Super-Kamiokande Collaboration, Phys. Rev. Lett. **81** 1158 (1998).
2) M. Nakahata *et al.*, Nucl. Instrum. Methods Phys. Res. Sect. A **421**, 113 (1999).
3) Super-Kamiokande Collaboration, Phys. Rev. Lett. **82**, 2430 (1999).

4) Y. Takeuchi *et al.*, Phys. Lett. **B452**, 418 (1999).
5) Super-Kamiokande Collaboration, Phys. Rev. Lett. **82**, 1810 (1999).
6) E. Blaufuss *et al.*, Nucl. Instrum. Methods Phys. Res. Sect. A **458**, 636 (2001).
7) Super-Kamiokande Collaboration, hep-ex/0103032.
8) Super-Kamiokande Collaboration, hep-ex/0103033.
9) J. N. Bahcall *et al.*, astro-ph/0010346.
10) C. E. Ortiz *et al.*, Phys. Rev. Lett. **85**, 2909 (2000).
11) B.T.Cleveland et al., Astrophys. J. **496**, 505 (1998).
12) V.Gavrin, Nucl. Phys. B(Proc. Suppl.) **91**, 36 (2001); J.N.Abdurashitov et al., Phys. Lett. B**328**, 234 (1994).
13) E.Bellotti, Nucl. Phys. B(Proc. Suppl.) **91**, 44 (2001); W.Hampel et al., Phys. Lett. B**388**, 364 (1996); P.Anselmann et al., Phys. Lett. B**342**, 440 (1995).